Journal of Power Sources 575 (2023) 233184

Contents lists available at ScienceDirect

Journal of Power Sources

journal homepage: www.elsevier.com/locate/jpowsour

Effects of an easy-to-implement water management strategy on performance and degradation of polymer electrolyte fuel cells

Shangwei Zhou [a], Linlin Xu [a,b], Panagiotis Trogadas [b], Lara Rasha [a], Wenjia Du [a], Paul R. Shearing [a], Marc-Olivier Coppens [b], Dan J.L. Brett [a], Rhodri Jervis [a,*]

[a] Electrochemical Innovation Lab, Department of Chemical Engineering, University College London, London, WC1E 7JE, United Kingdom
[b] Centre for Nature Inspired Engineering & Department of Chemical Engineering, University College London, London, WC1E 7JE, United Kingdom

HIGHLIGHTS

- Long-term performance for intermittent RH control is compared to constant RH control.
- TEM, XPS and SEM characterise Post-mortem MEAs to quantify the degradation.
- Local dynamic response during gas switching is captured by current density mapping.

ARTICLE INFO

Keywords:
Polymer electrolyte fuel cell (PEFC)
RH Control
Water management
Current density distribution mapping
Temperature distribution mapping
Performance degradation

ABSTRACT

Intermittent switching between wet and dry reactant gases during operation in a polymer electrolyte fuel cell (PEFC) can improve performance stability, alleviating the effects of flooding by controlling the water content within the system. However, lifetime durability may be affected due to membrane electrode assembly (MEA) boundary delamination and membrane damage. Two relative humidity (RH) control strategies were investigated, using electrochemical performance and MEA degradation as critical indicators. It was found that intermittent switching between wet and dry gases does not accelerate fuel cell degradation if the duration of the dry gas period is set reasonably (dry gases stops before the voltage reaches the apex of the hump). Additionally, current and temperature distribution mapping was utilised to capture the dynamic response between these transitional stages. The switching of dry gases first makes the current density distribution homogeneous, and the maximum current density is reduced subsequently. Then, the current density near the inlet keeps decreasing. Intermittent switching between wet and dry reactant gases is easy to implement and overcomes limitations in mass transfer at medium and high current densities.

1. Introduction

PEFCs have long been considered a next-generation power source for automotive and stationary applications. However, the intrinsic problem of water management remains a critical technical challenge, as a maintained water balance is required to ensure proton transfer through the membrane electrolyte and avoid excess liquid water impeding reactant gases flowing to the catalytic sites [1,2]. Reactant starvation at the active sites leads to power loss and carbon corrosion [3]. Thus, water management strategies are critical for performance reliability. They can be achieved by optimising fuel cell design and humidification control [4]. The effect of different flow field designs on water management has been widely investigated [5], including the effect of the number of channels [6], flow field structure [7,8], gas diffusion layer (GDL) properties [9–12], and MEA compression [13]. Collectively, these studies show that optimising fuel cell design can help transport and distribute liquid water and reactants.

In most cases, internal (shorting, wicking material) and external humidification (bubbling, columns, porous membranes) are adopted to humidify the membrane [14]. Internal humidification can reduce the weight and volume of the fuel cell system, but the stack temperature needs to be accurately controlled. External humidification, such as membrane-based humidification, allows for better control of the water levels and is effective under most operating conditions [15]. Raman

* Corresponding author.
E-mail address: rhodri.jervis@ucl.ac.uk (R. Jervis).

https://doi.org/10.1016/j.jpowsour.2023.233184
Received 31 October 2022; Received in revised form 3 April 2023; Accepted 8 May 2023
Available online 22 May 2023

et al. [16] demonstrated rapid and accurate humidity regulation by mixing dry and humidified gas streams, which involves complex algorithms and hardware. However, the fuel cell inlet manifold RH is susceptible to multiple factors, such as changes in environmental temperature and load demand, which may also cause RH fluctuations, making it challenging to control accurately [17–19]. For example, the reactant gases may cool after the humidifier device. Removing water inside the catalyst layer (CL) is challenging due to its porous structure [20], with a hydrogen purge being the usual method to prevent flooding and recover the output voltage. However, it has been shown that the fuel cell stack voltage only increases slightly around 10 s after purging [21], indicating that the purge is a temporary method to remove liquid water, and it has proven difficult and ineffective. The possibility of a recurrence of flooding is also not uncommon after a short period, while prolonging the purge time will decrease system efficiency. A cathode surge is another approach to water removal, which involves a momentary increase in the air/oxygen flow rate supplied to the cathode, which leads to a higher stoichiometry than normal. Typical cathode stoichiometry ranges from 1.5 to 3 and can be increased to 10 in 1–2 s under cathode surge [22].

Because water management issues are related to the fuel cell system's efficiency, performance and complexity, it would be ideal to actively control the amount of external water being introduced into the system by switching between dry and wet reactant gases and manipulating the time intervals. Liquid water in the flow field and GDL can be removed without affecting the water content in the membrane and then keep the output voltage fluctuating within a narrow range compared with constant humidity control [23]. However, Kang et al. [24] reported that wet/dry reactant gases repetition cycling leads to MEA boundary delamination and membrane damage. In-plane swelling leads to membrane failures during wet/dry conditions mentioned by Wycisk et al. [25]. Our study presented here focuses on the long-term effects of intermittent humidification on the performance and degradation of fuel cells, in which two cells with different RH control strategies are tested. Transmission electron microscopy (TEM) and X-ray photoelectron spectroscopy (XPS) are adopted to characterise the degradation quantitatively. The effectiveness of the wet/dry gas switching strategy for long-term applications is verified. The dynamic response of switching between dry and wet gases is studied by current density and temperature distribution mapping, revealing the leading causes of voltage fluctuations.

2. Experimental setup and procedure

For long-term testing, the single-cell PEFC has an active area of 25 cm^2 and operates on a commercial test station (850e Advanced Fuel Cell Test System, Scribner Associates). The in-house fabricated MEA consists of commercial gas diffusion electrodes (HyPLAT, South Africa) with a Pt loading of 0.4 mg cm^{-2} and the Nafion™ HP (DuPont) with a thickness of 20.3 μm, and the electrodes employ a Freudenberg H23C9 carbon paper with MPL (Freudenberg, Germany) and a hydrophobic treatment [26]. The MEAs were hot-pressed between two heated platens in a hot-press (Carver Inc., USA) at 150 °C for 3 min. An S++ PCB board (S++ Simulation Services) is placed between the cathode flow field and the current collector of another bespoke 100 cm^2 single cell to understand the dynamic change in the activated region when wet gases are switched to dry gases. The S++ device can map current density and temperature distributions in a 14 × 14 and 7 × 7 array, respectively. Each current contact segment has an area of 50.5 mm^2. The test bench used is the Greenlight G60 (Greenlight Innovation), with operating conditions identical to those in the Scriber setup. The cooling system is customer-built. Deionised water serves as the coolant, maintained at 60 °C and circulated through the back of the cathode flow field plate by Huber CC-1.

The RH of the reactants under wet conditions is 100%, whilst dry gases bypass the bubble humidifier and enter the fuel cell directly. Measurements are made at two constant current densities of 800 mA cm^{-2} (Ohmic region) and 1200 mA cm^{-2} (near mass transport limited region). The cells are operated at a temperature of 60 °C. Stoichiometries for hydrogen and air were 1.5 and 3, respectively. A Reference 3000 (Gamry Instruments) is used for impedance measurements with a frequency range of 0.1 Hz to 10 kHz.

When the reactants (hydrogen and air) switch from wet to dry, the dry gases absorb moisture in the flow channel and GDL [23]. A continued supply of dry gases will eventually result in the membrane drying out, and subsequently, the electrolyte impedance increases until the reaction cannot proceed. The duration of the wet and dry gases must be determined before the durability test. As illustrated in Fig. 1A, the cell voltage did not drop significantly within 20 min (from 800 s to 2000 s) at 800 mA cm^{-2}, suggesting a suitable time frame for the duration of introducing wet gases. On switching to dry gas and the current density reaching back to 800 mA cm^{-2}, there is a sharp rise in voltage and then a slow, near plateau-like increase, showing a typical hump shape (Fig. 1A inset). The time before the voltage peak was about 130 s. To avoid potential MEA dehydration [27], the dry gas duration was set to 40 s. At 1200 mA cm^{-2}, the duration of the period with dry gases was set to 15 s, considering the higher flow rate of reactants at higher current density is conducive to water removal. It is important to note that, due to the limitations of the test station, switching between dry and wet gases requires a period of zero current or at least a low electrical load, switching under high load will result in untimely supply of reactants which is come from the hysteresis of the 3-way solenoid vales. Therefore, the current density is required to decrease before switching gases, and set back after switching gases.

As illustrated in Fig. 1B, one set of experiments was conducted with wet/dry gases cycles at two different current densities (800 and 1200 mA cm^{-2}, RH-switching), as opposed to the other set of experiments with wet/wet gases cycles (RH-constant). The reason for not considering the activation region (low current densities region) is that fuel cells are mainly operated in the medium-to-high current densities region, and water management is more of a problem at higher operating current densities [28]. The 800 mA cm^{-2} testing duration is around 200 h (consisting of 520 cycles), and the 1200 mA cm^{-2} is around 50 h (consisting of 128 cycles). Electrochemical impedance spectroscopy (EIS) measurements were performed at the beginning and end of each current density test. To condition the MEA, 10 voltage sweeps were performed between open circuit voltage (OCV) and 0.3 V at 0.05 V increments for 10 s each. For the polarisation curve, voltage sweeps were performed between OCV and 0.4 V at 0.025 V increments for 30 s each.

For the post-mortem analysis, the cell fixture was opened post-operation, and the gaskets/GDLs were slowly removed from the MEAs to ensure that there were no cracks on the surface of CLs. TEM is conducted on a JEOL JEM-2100F electron microscope operated at 200 kV to characterise the size and morphology of the Pt/C catalysts from the unused and used 25 cm^2 MEAs (RH-switching and RH-constant). Pt/C catalysts are obtained from MEAs after the GDL is peeled off, and TEM is performed for all samples immediately after dispersing the Pt particles in methanol. The Pt/C catalyst powders were dispersed on the copper grid after being immersed in the methanol solution for less than 2 min. For the microscopic analyses, a drop of the particle solution is dispensed onto a 3 mm carbon-coated copper grid placed on an absorbent paper, and the grids, loaded with particles, are dried under ambient conditions. The TEM images are used to distinguish between individual and agglomerated particles, followed by segmentation and quantifying the particle size distribution of Pt using ImageJ software. XPS measurements are conducted to provide detailed information on the composition and chemical state of each element present on the surface of the CL. A survey scan between 0 and 1200 eV is performed for each sample (2 × 2 cm^2). Then, high-resolution scans for carbon, fluorine, oxygen, platinum, and sulphur are conducted with 20 eV pass energy. CasaXPS software is used for data processing. The peak area ratio of the Pt 4f doublet ($f_{5/2}$: $f_{7/2}$) is fixed to 3: 4, and for the S 2p doublet ($p_{1/2}$: $p_{3/2}$) is fixed to 1 : 2.

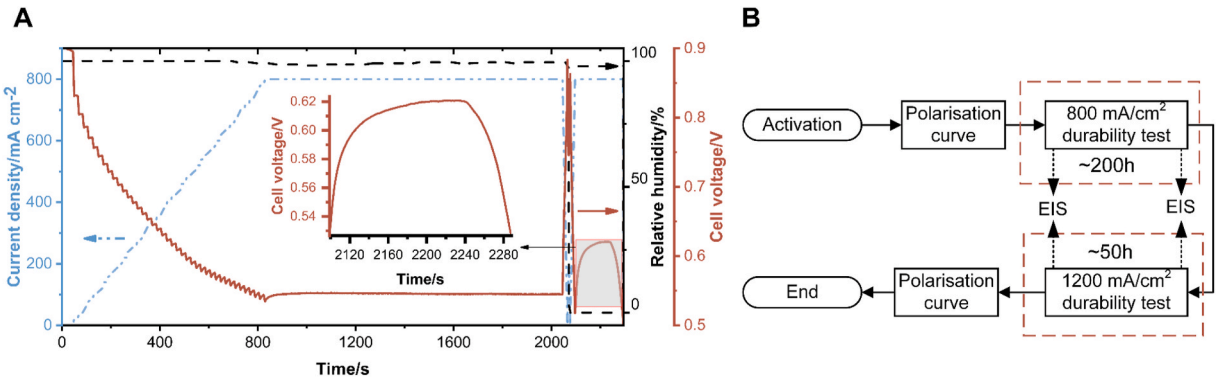

Fig. 1. (A) Evolution of cell voltage (red) when wet gases are switched to dry gases at 800 mA cm^{-2} for the 25 cm^2 cell. (B) Experimental protocol in Scribner 850e: comparing different RH control strategies at two constant current densities. (For interpretation of the references to colour in this figure legend, the reader is referred to the Web version of this article.)

3. Results and discussion

3.1. Voltage evolution and impedance analysis

Fig. 2A and B shows the voltage evolution at 800 mA cm^{-2}, where the voltage oscillation indicates the period of EIS measurement. Since the transient voltage fluctuation is caused by the load change to achieve gas switching, we mainly focus on the long-term voltage change under different gas cycles. When wet gases were supplied after the activation process, the initial voltage of the RH-constant cell was ~0.633V, which is higher than the ~0.622V of the RH-switching cell. The slight difference in the initial voltage could be due to inconsistencies in the MEA manufacturing process or cell assembly. After about 200 h of long-term testing, the voltage of the RH-switching cell increased to ~0.647 V. This is a 4% improvement in performance at 800 mA cm^{-2} compared to the initial point. This voltage increase is primarily due to an intermittent dry gases supply that provides the cell with optimal water balance, allowing reactants to reach the CL with less obstruction throughout the long-term test. Also, as will be shown further on in Fig. 7A, the pressure drop is reduced at both the anode and cathode when switching to the dry gases, indicating that the liquid water in the flow field and GDL is effectively removed. For RH-constant cell (wet/wet gases cycled), the voltage continually decreases to ~0.595V because of continuous water accumulation. Fig. 3A and B shows the corresponding voltage evolution at 1200 mA cm^{-2}. The voltages of both cells decreased from ~0.564 V and ~0.559 V to ~0.551 V and ~0.537 V, respectively. These drops correspond to 2% and 4%, respectively. No voltage increase was observed compared with the performance at 800 mA cm^{-2}. However, the voltage decline of the RH-switching cell is lower. This indicates that the intermittent switching between wet and dry gases can reduce the rate of cell voltage degradation, but the duration of flowing wet and dry gases needs to be optimised for the higher current density to improve cell

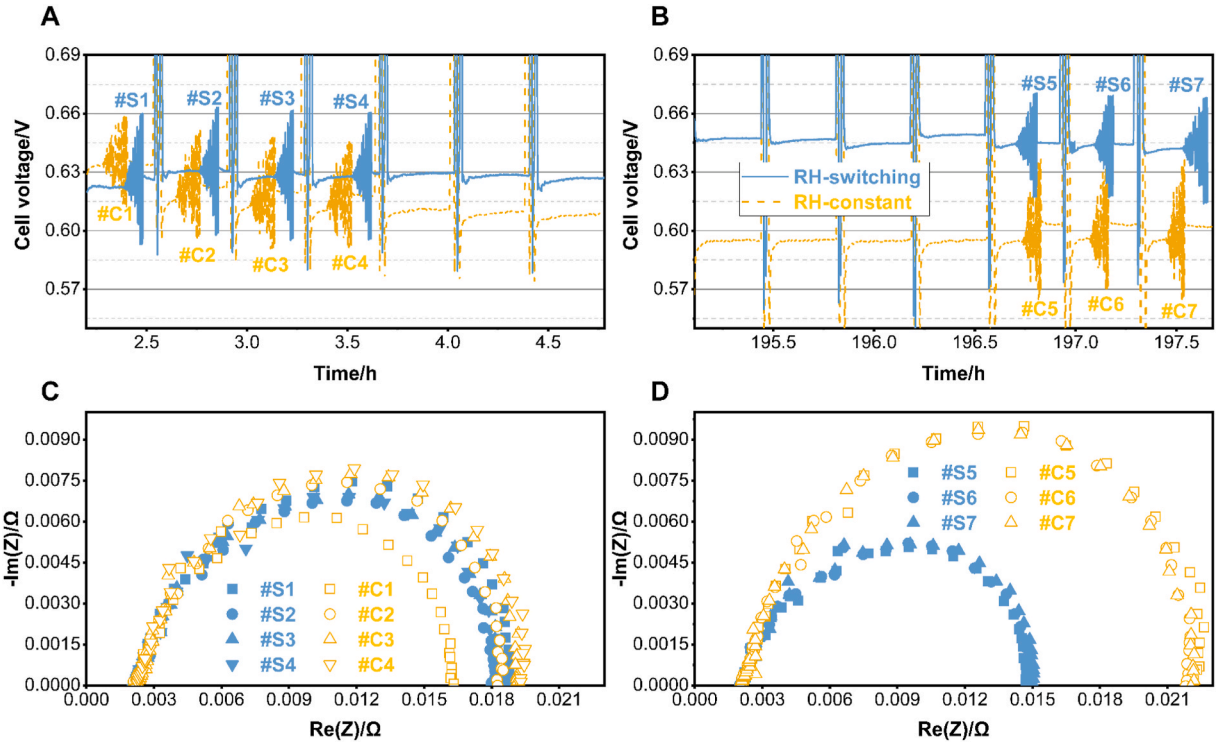

Fig. 2. Voltage evolution (A, B) and EIS measurement (C, D) at the beginning and end of the 800 mA cm^{-2} long-term test. 'S' represents RH-switching with wet/dry gases cycles (blue), and 'C' is RH-constant with wet/wet gases cycles (yellow). (For interpretation of the references to colour in this figure legend, the reader is referred to the Web version of this article.)

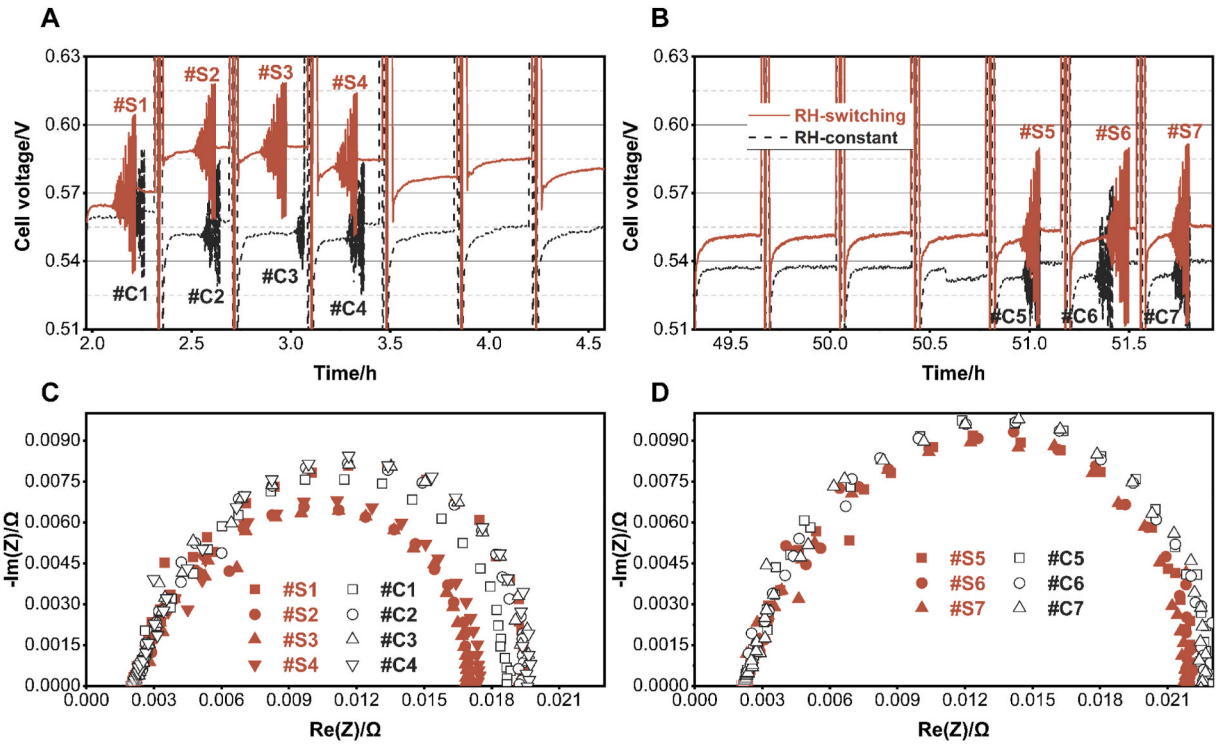

Fig. 3. Voltage evolution (A, B) and EIS measurements (C, D) at the beginning and end of the 1200 mA cm^{-2} durability test. (red), S′ represents RH-switching and 'C' is RH-constant (black). (For interpretation of the references to colour in this figure legend, the reader is referred to the Web version of this article.)

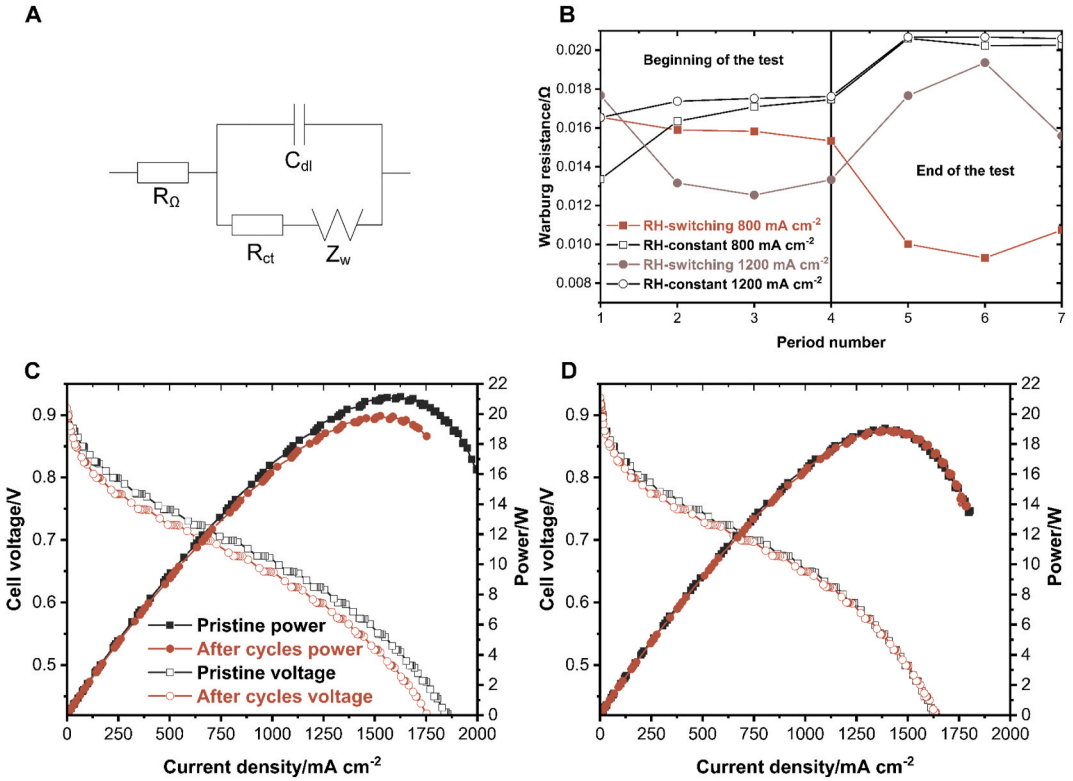

Fig. 4. (A) The Randle's equivalent circuit model; (B) Warburg resistance fitting results for EIS measurements. Overall performance before and after the durability test; (C) RH-constant and (D)RH-switching.

performance. The load reduction of switching gas impacts fuel cell performance, so the load reduction is also retained in wet/wet gases cycles.

When the wet gases are switched to dry for the first time at each current density, the cell impedance decreases (#S1 to #S2 in Fig. 2C), especially in the low-frequency area; the impedance of the second

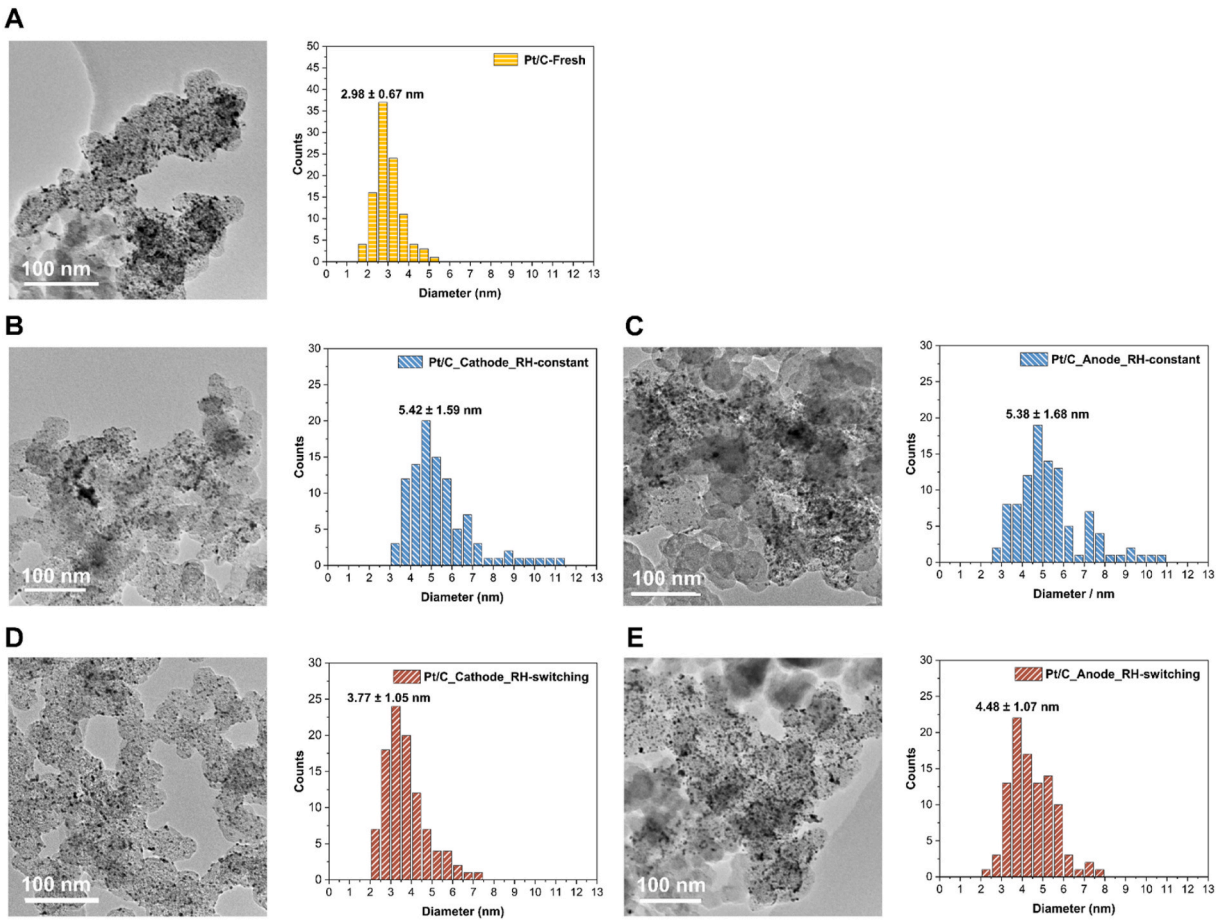

Fig. 5. TEM images and corresponding Pt particle size distributions for (A) fresh catalyst, (B, C) cathode and anode catalyst after testing with RH-constant cycles, (D, E) cathode and anode catalyst after testing with RH-switching cycles.

intersection with the real axis (R_i) decreases from 0.0187Ω to 0.0180Ω. Mass transport limitations are observed at lower frequencies because it takes time for the reactants to reach the catalyst sites. This indicates that the dry gases facilitate excess water removal and improve the mass transfer process. As shown in Fig. 2D, the impedance at the end of the 800 mA cm^{-2} durability test decreases (R_i falls to 0.0150Ω), meaning that the dry gases duration of 40 s is sufficient to achieve a good water balance. The impedance increases at the end of the 1200 mA cm^{-2} durability test (Fig. 3D); therefore, 15 s is insufficient to remove excess water, considering the significant amount of water production at this current density. The impedance increases at any current density for the RH-constant cell without effective water removal. Besides, the impedance for the RH-constant cell is always higher than the RH-switching one. The high-frequency intercept with the real axis represents the total Ohmic losses. It can be observed that the intermittent wet/dry gases switching can keep the membrane in proper hydration conditions (the total Ohmic losses is maintained at 0.002 Ω), and there is little difference compared to the supply of wet/wet gases. Therefore, any change in cell voltage can be attributed to water management in the flow fields, GDL and CL.

The Randles equivalent circuit model [29] shown in Fig. 4A is used to interpret the impedance results labelled by #S1-#S7 and #C1-#C7. Total Ohmic losses R_Ω represents the sum of contact and membrane resistance. R_{ct} models the charge transfer resistance that accounts for the cathode activation loss. C_{dl} represents the double-layer capacitance. The finite Warburg element Z_W models the mass transfer/diffusion process at low frequencies. As illustrated in Fig. 4B, the Warburg resistance of the RH-switching cell decreases at 800 mA cm^{-2}, while that of the RH-constant cell increases. This difference could be the result of accumulated liquid water, which affects the transport of reactants by blocking the pores in the GDE and CL, while the dry gases decrease the diffusion resistance by the periodic removal of this water. For 1200 mA cm^{-2}, the mass transfer resistance of both cells increases, which is consistent with the trend of the voltage evolution.

The cell's overall performance before and after the durability test are shown in Fig. 4C and D. For the RH-switching cell, the limiting current density and the maximum power do not significantly decline (Fig. 4D); however, for the RH-constant cell, the output voltage declined at all polarisation regions after the long-term test (Fig. 4C). The liquid water is removed with intermittent wet and dry gases switching, and a higher limiting current density can be reached due to a reduction in mass transport limitations. Based on the results of around 250 h of long-term testing, it can be concluded that wet/dry gas cycles do not accelerate MEA degradation for the set dry gases durations.

3.2. *Post-mortem analysis*

The MEA samples analysed prior to fuel cell operation are referred to as "fresh MEA", whereas samples tested post-fuel cell operation with or without gas switching are referred to as "used MEA_RH-s adjacent orientation witching" and "used MEA_RH-constant", respectively. Fig. 5 shows the TEM images of the fresh and used Pt/C catalysts, which present the morphological changes and particle size distribution of Pt/C catalysts in the cathode and anode. On the right side of each micrograph are the histograms showing the average size and distributions of the Pt particles within randomly chosen areas in the TEM image containing 100 nanoparticles each. As exhibited in Fig. 5A, the morphology of the catalysts from hot-pressed but fresh MEA is well-dispersed with

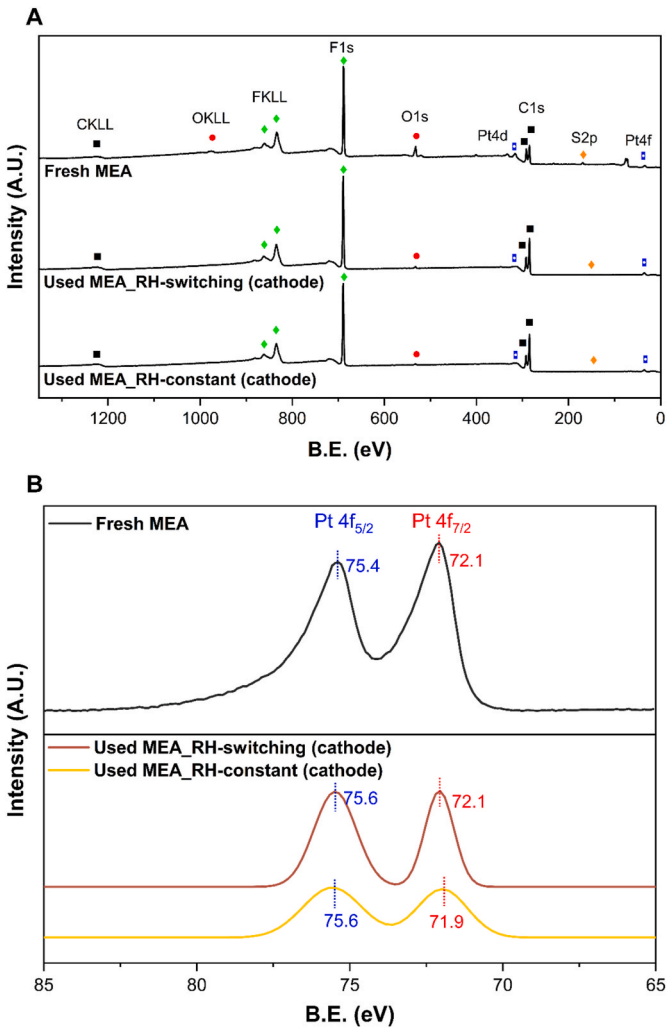

Fig. 6. (A) XPS survey spectra of the cathode side of fresh and used MEAs. (B) XPS Pt4f spectra of the cathode of fresh and used MEAs.

nanosized Pt nanoparticles (ca. 2.98 nm) onto the carbonaceous support. After long-term PEFC operation with and without gas switching, individual Pt particles grow larger, with spherical particles being observed to have a certain degree of agglomeration, resulting in broader size distribution. The increased size of the Pt particles after PEFC operation was caused by Ostwald ripening to reach a more thermodynamically stable state, wherein the surface-area-to-volume ratio is minimised. This process has been shown to be unavoidable due to the observance of the local dissolution of small Pt^0 particles and precipitation of the dissolved Pt^{2+} species [30]. Besides, the carbon corrosion around the Pt causes its eventual detachment from the support and consequent migration and merging to form a bigger particle. It is interesting to note that the growth of Pt particles in the anode shows a similar growth level as in the cathode (similar to the TEM results of Kim et al. [3]), as carbon corrosion can happen both in the cathode and anode. The Pt particles were measured to have average diameters of ca. 5.42 nm and ca. 5.38 nm for the cathode and anode of the used MEA with RH-constant cycles (Fig. 5B and C). The size of the Pt particles after the fuel cell was tested with intermittent wet/dry gas switching was much smaller in comparison, with average diameters of ca. 3.77 nm and ca. 4.48 nm for the cathode and anode (Fig. 5D and E). This happened due to the faster Pt particle growth with increasing RH, especially during potential cycling [31]. For RH-constant cycled cell, because water is generated on the cathode side, the Pt particles of the cathode side are slightly larger than at the anode. However, the wet/dry gas cycled cell shows the opposite, possibly due to the high stoichiometry at the cathode, accompanied by strong water removability. For the RH-switching cycled cell, there is a balance between reduced utilisation and reduced mass transfer resistance due to the increase in Pt particle size [32]. The cell performance does not degrade significantly, though one could assume that these early indicators of degradation could cause more critical performance loss as they proceed to a point where the loss in ECSA becomes critical and that the discrepancy in degradation between the two humidification strategies here will cause divergent and significant performance loss with longer duration testing.

XPS measurements of samples from the anode and cathode were conducted to quantify the chemical changes of elements on the CL. XPS survey scans (Fig. 6A and S1) demonstrate the presence of carbon (C), oxygen (O), fluorine (F), sulphur (S), and platinum (Pt) on the surface of all CL samples before and after fuel cell operation.

The carbon spectrum of fresh MEA (Fig. S2) shows two dominant peaks at ~284.9 and ~292 eV, assigned to graphitic carbon and fluorinated carbon (CF_x, x = 1,2,3) in the ionomer, respectively. An additional minor peak at ~285 eV represents an oxidised form of carbon (C–O). After fuel cell operation, the intensity of the fluorinated carbon peak is significantly decreased for both samples (Figs. S3 and S4), implying a decrease in the surface concentration of the ionomeric forms of carbon relative to the graphitic forms of carbon. This observation is confirmed by the calculated ratio of fluorinated/graphitic carbon ($\sum fluorinated\ C / \sum graphitic\ C$) in each sample, demonstrating that the decrease in fluorinated carbon is due to ionomer degradation and dissolution during long-term operation (Table 1); the concentration of CF_2 species in the "used MEA" samples is increased due to the dissolution of CF_3 species [33].

Ionomer degradation is also confirmed by the F, S, and O spectra of the MEA samples before and after fuel cell operation. F spectra (Figs. S5–7) are associated with Nafion® polymer; the two peaks at ~689 eV and ~691 eV correspond to the hydrophobic CF_x groups in the Nafion® backbone and the other fluorine-containing groups (-OCF) in the pendant side chain of Nafion®, respectively [33,34]. The total surface concentration of fluorine decreases by ~9% and 5% post fuel cell operation without and with gases switching (Table 2); hence, the CL becomes less hydrophobic due to the decomposition of CF_x groups.

Furthermore, the O spectra (Figs. S8–10) confirm the significant loss of sulphonic acid groups (-S═O) from the ionomer during fuel cell operation since there is a ~98% and ~95% loss after fuel cell operation without and with gases switching, respectively (Table 3). The S 2p spectra confirm this of fresh and used MEA samples related to the sulphur species in the ionomer (Figs. S11–13); their surface concentration is diminished after fuel cell operation. On the contrary, the percentage of oxidised elements (C, Pt) on the surface of the CL is increased by 50% due to the oxidation of carbonaceous support and Pt (Table 3).

Thus, the partial loss of ionomer from the surface of the CL affects its hydrophobicity and proton conductivity, as the non-uniform ionomer film thickness was created across the CL regions. Thicker ionomer layers generate higher oxygen transport, and thinner ionomer layers exhibit higher proton conduction resistances, which results in an inevitable loss in PEFC performance (Fig. 4C) [35,36]. Additionally, the presence of excess ionomer in some regions of the CL can block the nanopores of the support and decrease the interparticle distance between the Pt particles located within, reducing the electrochemically active surface area and enhancing Ostwald ripening, respectively [37]. Finally, the higher acid (H_2SO_4) concentration in the thicker ionomer regions can be associated with higher Pt solubility, leading to increased Pt agglomeration [38]. Pt spectra (Fig. 6A and S1, Fig. 6B and S14) show that metallic and oxidised species are present on the surface of the CL. The presence of Pt $4d_{5/2}$ at ~315 eV (Fig. 6A and S1) and its doublet Pt $4d_{3/2}$ at ~333 eV correspond to metallic Pt (Pt^0) [39,40], whereas Pt 4f doublet peaks at ~ 72.1 ($4f_{7/2}$) and ~75.4 ($4f_{5/2}$) eV are assigned to oxidised platinum [34]. Even though there are no changes in the binding energy for the fresh and used MEA samples, a significant decrease in the signal intensity of the

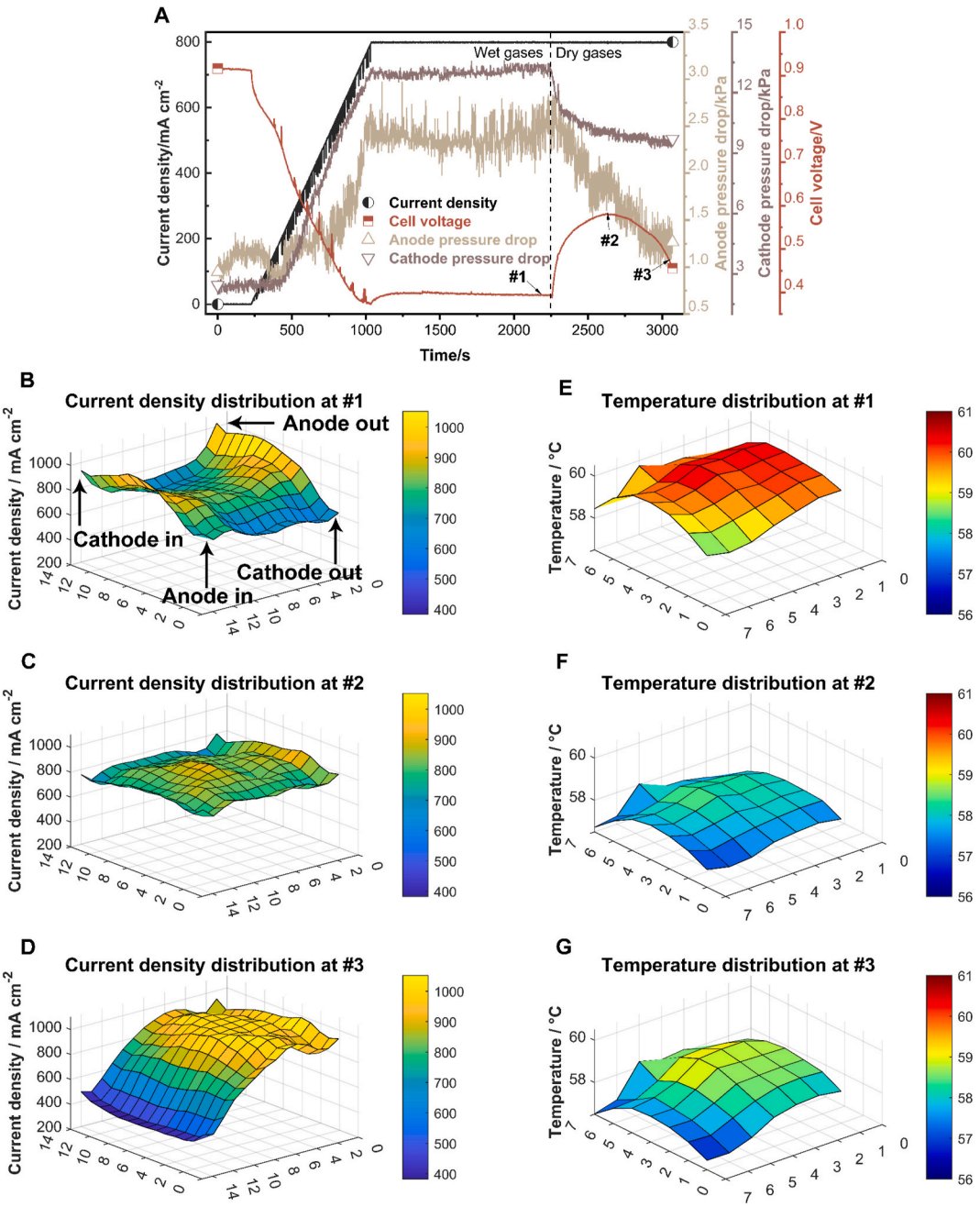

Fig. 7. (A) Evolution of cell voltage and pressure drop when wet gases are switched to dry gases, data collected from Greenlight G60. (B–D) Current density (x and y axes represent measurement array 1–14) and (E–G) temperature distribution mapping (x and y axes represent measurement array 1–7) at #1, #2 and #3.

used MEA samples is revealed (Table 3). It is consistent with previous reports in the literature [41] and indicates the accelerated degradation of Pt and its migration at the interface between the CL and the polymer electrolyte membrane [30].

These XPS results demonstrate that fuel cell operation with wet/wet gases switching causes more significant degradation of the CL than fuel cell operation with wet/dry gases switching. Under all experimental conditions tested, the degradation of the cathode CL is more severe than its counterpart at the anode due to the generated and accumulated water at the cathode. This excess quantity of water causes local oxidant starvation and, hence, high local potential, resulting in carbon corrosion and dissolution of Pt, as also evidenced by the TEM results [41,42]. Figs. S15–S17 show scanning electron microscope (SEM) images of the fresh and used MEA in cross-section. We do not see evidence of delamination in any of the SEM cross-sections, which proved that the intermittent gas swathing protocol does not result in MEA boundary delamination and membrane damage compared to constant RH. Moreover, the fact that neither of the two procedures that we compare here cause delamination at this point in the testing allows us to attribute the performance degradation to the catalysts only at this stage in the aging.

3.3. Dynamic response

In order to assess the local dynamic response during gas switching, a different test station was required that enabled switching of gases without reducing the current. A 100 cm^2 segmented current and temperature measurement device was used for these experiments, meaning the results presented in this section are from larger MEAs than in the durability testing. As shown in Fig. 7A, the cell voltage also shows a characteristic hump shape after switching from wet gases to dry gases

Table 1
XPS chemical state information obtained from the C spectrum of the MEAs before (Fresh MEA) and after the long-term test (RH-constant and RH-switching).

C chemical state	C composition (atomic %)					
	Fresh MEA		Used MEA RH-constant		Used MEA RH-switching	
	cathode	anode	cathode	anode	cathode	anode
Graphitic C	29.9	32.1	39.0	41.1	40.6	43.2
CF	21.2	13.6	14.9	15	12.7	12.8
CF_2	22.7	25.6	19.1	17.9	21.8	19.3
CF_3	2.8	0.6	0.0	0.0	0.0	0.0
C–O	23.4	28.1	27	26	24.9	24.7
Total	100	100	100	100	100	100
The ratio of fluorinated/ graphitic C	1.56	1.24	0.87	0.80	0.85	0.74

Table 2
Elemental composition of the MEAs before (Fresh MEA) and after the long-term test (RH-constant and RH-switching).

Element	Elemental composition (atomic %)					
	Fresh MEA		Used MEA RH-constant		Used MEA RH-switching	
	cathode	anode	cathode	anode	cathode	anode
C	15.4	15.3	35.4	33.5	32.1	30.5
F	61.7	61.8	56	57.7	58.9	60.8
O	7.8	7.8	1.1	1.4	1.3	1.4
Pt	14.2	14.2	7.5	7.4	7.7	7.3
S	0.9	0.9	0.0	0.0	0.0	0.0
Total	100	100	100	100	100	100

Table 3
XPS chemical state information obtained from the O and Pt spectrum of the MEAs before (Fresh MEA) and after the long-term test (RH-constant and RH-switching).

Element Species	O and Pt composition (atomic %)		
	Fresh MEA	Used MEA RH-constant	Used MEA RH-switching
-S═O	50	0.7	1.6
Oxidised elements (C, Pt)	50	99.3	98.4
Pt(cathode)	14.2	7.5	7.7
Pt(anode)	14.2	7.3	7.3

for the cell with a larger active area. The voltage at 800 mA cm^{-2} before gas switching is 0.395 V (marked #1 in Fig. 7A) and continues to increase up to 0.581V (#2) after the switch. During this process, the pressure drop at the cathode presents a rapid decrease, and the pressure drop at the anode side gradually decreases, which indicates that the flow resistance decreases, with the cell voltage ultimately dropping to 0.475V at #3. Analysing the current density distribution mapping can explain the hump-shaped voltage variation.

It can be observed from Fig. 7B that the current density at the cathode outlet is low at #1, because the water generated by the oxygen reduction reaction (ORR) will accumulate at the outlet as it moves along the flow channel. The membrane at the cathode inlet has optimal water content, and the area is least affected by water accumulation, which results in a relatively higher current density.

The supply of dry gases results in water and effective heat removal in the cell, allowing a relatively uniform distribution of the reactants over the active area (Fig. 7C and F). It indicates that the homogeneous reaction is advantageous for the even distribution of temperature. However, overly long exposures to dry gases will eventually cause the membrane at the air inlet to dehydrate, and the protons produced at the anode cannot be transported through the membrane. Because of this, the ORR will occur mainly at the cathode outlet (Fig. 7D). It can also be seen from the temperature distribution (Fig. 7G) that the temperature at the outlet is higher than at the inlet because of the higher reaction rate.

The analytics results from Fig. 7B–G are presented in Table 4 to explain the higher voltage in #2. The distribution of the highest current density at #1 and #3 is higher than at #2. According to the polarisation curve, higher current density inevitably leads to lower voltage. Moreover, the uneven distribution of current density tends to lead to an inhomogeneous temperature distribution, and the average temperature at #1 and # 3 is higher than that at #2 (Fig. 7E–G). It should be noted that the average temperature at #1 is higher than at #3, since the cooling flow channel is on the back of the anode flow field plate, and the coolant temperature is set to 60 °C. The water content in the cell is relatively high at #1 compared to #3 because the decrease in pressure drop indicates the removal of water, and water is also a more effective conductor of heat than air. Therefore, the temperature at #1 is close to 60 °C. At the same time, the standard deviation of the current density at #2 is only 48.7 mA cm^{-2}, which is relatively homogenous, and the degradation of the whole MEA will be consistent.

4. Conclusion

Intermittent wet and dry gases switching is beneficial to relieve water flooding and maintain the water content in the membrane at an appropriate level. Additionally, it does not cause a decrease in system efficiency compared to a purge or surge. After about 250 h of long-term testing, the RH-switching cell with wet and dry gases switching remained stable, while the RH-constant cell without dry gases switching showed a significant voltage decrease over the entire current density range. This is backed by the post-mortem TEM analysis, showing a similar trend. The diameters of Pt particles on the cathode and anode of the RH-switching cell are ca. 3.77 nm and ca. 4.48 nm, respectively, while the particle sizes of another cell are 5.42 nm and ca. 5.38 nm, which shows more obvious aggregation. XPS results also indicate that MEAs of RH-constant cell cause more significant degradation of the CL than RH-switching cell. We acknowledge that different degradation modes, such as delamination among the membrane, CLs and GDL, may present themselves on longer-duration testing, suggesting follow-on studies to look at long-term durability or ASTs and the effect on delamination of humidity switching.

The switching of dry gases makes the distribution of current density homogeneous and reduces the maximum current density. After removing liquid water, the reactants can reach the entire active area and the cell voltage increases. Nevertheless, the voltage drops when the dry gases are continually supplied, and the proton transfer is mainly carried out at the cathode outlet. The duration of the wet gases determines the accumulation of water, while the duration of the dry gases determines their expulsion. These two factors suggest a new way to achieve optimal water management in a PEFC. In the future, the advanced instrumentation of this cell could be used to build data-driven models that provide adaptive RH switching based on simpler signals, such as an AC voltage response [43] or current density distribution.

Table 4
Descriptive analytics of current density and temperature distribution mapping at different times (#1, #2 and #3).

	#1	#2	#3
Maximum current density, mA cm^{-2}	1051.3	916.7	1040.4
Minimum current density, mA cm^{-2}	621.5	669.7	383.4
Current density distribution standard deviation, mA cm^{-2}	99.4	48.7	211.1
Average temperature, °C	59.7	57.8	58.0
Temperature distribution standard deviation, °C	0.5	0.4	0.6

CRediT authorship contribution statement

Shangwei Zhou: Conceptualization, Methodology, Formal analysis, Investigation, Data curation, Writing – original draft, Writing – review & editing, Visualization. **Linlin Xu:** Formal analysis, Investigation, Data curation, Visualization, Visualization, Writing - original draft, Writing - review & editing. **Panagiotis Trogadas:** Formal analysis, Writing – original draft, Writing – review & editing, Visualization. **Lara Rasha:** Writing – original draft, Writing – review & editing. **Wenjia Du:** Writing – original draft, Writing – review & editing. **Paul R. Shearing:** Resources, Writing – review & editing, Funding acquisition. **Marc-Olivier Coppens:** Resources, Writing – review & editing, Supervision, Funding acquisition. **Dan J.L. Brett:** Resources, Writing – review & editing, Supervision, Funding acquisition. **Rhodri Jervis:** Conceptualization, Resources, Writing – original draft, Writing – review & editing, Supervision, Project administration, Funding acquisition.

Declaration of competing interest

The authors declare that they have no known competing financial interests or personal relationships that could have appeared to influence the work reported in this paper.

Data availability

Data will be made available on request.

Acknowledgements

SZ acknowledges the Chinese Scholarship Council (CSC) for funding support of his PhD [grant number: 202108060113]. LX acknowledges the Engineering and Physical Sciences Research Council [grant number EP/N509577/1, EP/T517793/1] for funding support of her PhD. DB/PRS acknowledge the EPSRC for funding fuel cell research in the EIL (EP/L015277/1, EP/P009050/1, EP/M014371/1, EP/M009394/1, EP/M023508/1, EP/L015749/1, EP/N022971/1) and the Royal Academy of Engineering for supporting the Research Chairs of DB (RCSRF2021/13/53) and PRS (CiET1718/59). MOC is grateful to the EPSRC for funding via a "Frontier Engineering: Progression" grant (EP/S03305X/1). This project was supported by the Royal Academy of Engineering under the Research Chairs and Senior Research Fellowships scheme.

Appendix A. Supplementary data

Supplementary data to this article can be found online at https://doi.org/10.1016/j.jpowsour.2023.233184.

References

[1] J.P. Owejan, J.J. Gagliardo, J.M. Sergi, S.G. Kandlikar, T.A. Trabold, Water management studies in PEM fuel cells, Part I: fuel cell design and in situ water distributions, Int. J. Hydrogen Energy 34 (2009) 3436–3444.
[2] X. Wang, Y. Ma, J. Gao, T. Li, G. Jiang, Z. Sun, Review on water management methods for proton exchange membrane fuel cells, Int. J. Hydrogen Energy 46 (2021) 12206–12229.
[3] M. Kim, N. Jung, K. Eom, S.J. Yoo, J.Y. Kim, J.H. Jang, et al., Effects of anode flooding on the performance degradation of polymer electrolyte membrane fuel cells, J. Power Sources 266 (2014) 332–340.
[4] H. Li, Y. Tang, Z. Wang, Z. Shi, S. Wu, D. Song, et al., A review of water flooding issues in the proton exchange membrane fuel cell, J. Power Sources 178 (2008) 103–117.
[5] B. Lim, E. Majlan, W. Daud, T. Husaini, M.I. Rosli, Effects of flow field design on water management and reactant distribution in PEMFC: a review, Ionics 22 (2016) 301–316.
[6] Y. Wu, J. Cho, T. Neville, Q. Meyer, R. Ziesche, P. Boillat, et al., Effect of serpentine flow-field design on the water management of polymer electrolyte fuel cells: an in-operando neutron radiography study, J. Power Sources 399 (2018) 254–263.
[7] V. Bethapudi, J. Hack, P. Trogadas, J. Cho, L. Rasha, G. Hinds, et al., A lung-inspired printed circuit board polymer electrolyte fuel cell, Energy Convers. Manag. 202 (2019), 112198.
[8] P. Trogadas, J. Cho, T. Neville, J. Marquis, B. Wu, D. Brett, et al., A lung-inspired approach to scalable and robust fuel cell design, Energy Environ. Sci. 11 (2018) 136–143.
[9] P.K. Sinha, P.P. Mukherjee, C.-Y. Wang, Impact of GDL structure and wettability on water management in polymer electrolyte fuel cells, J. Mater. Chem. 17 (2007) 3089–3103.
[10] S. Park, B.N. Popov, Effect of hydrophobicity and pore geometry in cathode GDL on PEM fuel cell performance, Electrochim. Acta 54 (2009) 3473–3479.
[11] K. Zhou, T. Li, Y. Han, J. Wang, J. Chen, K. Wang, Optimizing the hydrophobicity of GDL to improve the fuel cell performance, RSC Adv. 11 (2021) 2010–2019.
[12] A. Kakaee, G. Molaeimanesh, M.E. Garmaroudi, Impact of PTFE distribution across the GDL on the water droplet removal from a PEM fuel cell electrode containing binder, Int. J. Hydrogen Energy 43 (2018) 15481–15491.
[13] N. Kulkarni, J.I. Cho, L. Rasha, R.E. Owen, Y. Wu, R. Ziesche, et al., Effect of cell compression on the water dynamics of a polymer electrolyte fuel cell using in-plane and through-plane in-operando neutron radiography, J. Power Sources 439 (2019), 227074.
[14] Y. Chang, Y. Qin, Y. Yin, J. Zhang, X. Li, Humidification strategy for polymer electrolyte membrane fuel cells–A review, Appl. Energy 230 (2018) 643–662.
[15] F. Migliardini, A. Unich, P. Corbo, Experimental comparison between external and internal humidification in proton exchange membrane fuel cells for road vehicles, Int. J. Hydrogen Energy 40 (2015) 5916–5927.
[16] S. Raman, S. Swaminathan, S. Bhardwaj, H.K. Tanneru, B. Bullecks, R. Rengaswamy, Rapid humidity regulation by mixing of dry and humid gases with feedback control for PEM fuel cells, Int. J. Hydrogen Energy 44 (2019) 389–407.
[17] H. Fu, J. Shen, L. Sun, K.Y. Lee, Fuel cell humidity modeling and control using cathode internal water content, Int. J. Hydrogen Energy 46 (2021) 9905–9917.
[18] X. Chen, J. Xu, Q. Liu, Y. Chen, X. Wang, W. Li, et al., Active disturbance rejection control strategy applied to cathode humidity control in PEMFC system, Energy Convers. Manag. 224 (2020), 113389.
[19] Y. Song, X. Wang, AI-based proton exchange membrane fuel cell inlet relative humidity control, IEEE Access 9 (2021) 158496–158507.
[20] Y. Tang, J. Zhang, C. Song, H. Liu, J. Zhang, H. Wang, et al., Temperature dependent performance and in situ AC impedance of high-temperature PEM fuel cells using the Nafion-112 membrane, J. Electrochem. Soc. 153 (2006), A2036.
[21] M. Song, P. Pei, H. Zha, H. Xu, Water management of proton exchange membrane fuel cell based on control of hydrogen pressure drop, J. Power Sources 267 (2014) 655–663.
[22] J.B. Siegel, S.V. Bohac, A.G. Stefanopoulou, S. Yesilyurt, Nitrogen front evolution in purged polymer electrolyte membrane fuel cell with dead-ended anode, J. Electrochem. Soc. 157 (2010), B1081.
[23] I. Hussaini, C. Wang, Dynamic water management of polymer electrolyte membrane fuel cells using intermittent RH control, J. Power Sources 195 (2010) 3822–3829.
[24] J. Kang, J. Kim, Membrane electrode assembly degradation by dry/wet gas on a PEM fuel cell, Int. J. Hydrogen Energy 35 (2010) 13125–13130.
[25] R. Wycisk, P.N. Pintauro, J.W. Park, New developments in proton conducting membranes for fuel cells, Current Opinion in Chemical Engineering 4 (2014) 71–78.
[26] J. Hack, P.A. García-Salaberri, M.D. Kok, R. Jervis, P.R. Shearing, N. Brandon, et al., X-ray micro-computed tomography of polymer electrolyte fuel cells: what is the representative elementary area? J. Electrochem. Soc. 167 (2020), 013545.
[27] K.R. Minard, V.V. Viswanathan, P.D. Majors, L.-Q. Wang, P.C. Rieke, Magnetic resonance imaging (MRI) of PEM dehydration and gas manifold flooding during continuous fuel cell operation, J. Power Sources 161 (2006) 856–863.
[28] J. Shen, L. Xu, H. Chang, Z. Tu, S.H. Chan, Partial flooding and its effect on the performance of a proton exchange membrane fuel cell, Energy Convers. Manag. 207 (2020), 112537.
[29] N. Fouquet, C. Doulet, C. Nouillant, G. Dauphin-Tanguy, B. Ould-Bouamama, Model based PEM fuel cell state-of-health monitoring via ac impedance measurements, J. Power Sources 159 (2006) 905–913.
[30] P. Trogadas, J.I. Cho, N. Kapil, L. Rasha, A. Corredera, D.J. Brett, et al., Effect of extended short-circuiting in proton exchange membrane fuel cells, Sustain. Energy Fuels 4 (2020) 5739–5746.
[31] W. Schmittinger, A. Vahidi, A review of the main parameters influencing long-term performance and durability of PEM fuel cells, J. Power Sources 180 (2008) 1–14.
[32] J. Zhang, Y. Wang, P. Cao, J. Lu, J. Zhang, A new discovery of the active impact of Pt/C particles aggregation on electrode performance in PEMFC, Int. J. Hydrogen Energy 42 (2017) 527–534.
[33] F.-Y. Zhang, S.G. Advani, A.K. Prasad, M.E. Boggs, S.P. Sullivan, T.P. Beebe Jr., Quantitative characterization of catalyst layer degradation in PEM fuel cells by X-ray photoelectron spectroscopy, Electrochim. Acta 54 (2009) 4025–4030.
[34] V. Parry, G. Berthomé, J.-C. Joud, O. Lemaire, A.A. Franco, XPS investigations of the proton exchange membrane fuel cell active layers aging: characterization of the mitigating role of an anodic CO contamination on cathode degradation, J. Power Sources 196 (2011) 2530–2538.
[35] G. Doo, J.H. Lee, S. Yuk, S. Choi, D.-H. Lee, D.W. Lee, et al., Tuning the ionomer distribution in the fuel cell catalyst layer with scaling the ionomer aggregate size in dispersion, ACS Appl. Mater. Interfaces 10 (2018) 17835–17841.
[36] A. Orfanidi, P. Madkikar, H.A. El-Sayed, G.S. Harzer, T. Kratky, H. Gasteiger, The key to high performance low Pt loaded electrodes, J. Electrochem. Soc. 164 (2017) F418.
[37] A. Kobayashi, T. Fujii, C. Harada, E. Yasumoto, K. Takeda, K. Kakinuma, et al., Effect of Pt and ionomer distribution on polymer electrolyte fuel cell performance and durability, ACS Appl. Energy Mater. 4 (2021) 2307–2317.

[38] R. Shimizu, Y.-C. Park, K. Kakinuma, A. Iiyama, M. Uchida, Effects of both oxygen permeability and ion exchange capacity for cathode ionomers on the performance and durability of polymer electrolyte fuel cells, J. Electrochem. Soc. 165 (2018), F3063.
[39] X. Wang, H. Yu, D. Hua, S. Zhou, Enhanced catalytic hydrogenation activity and selectivity of Pt-M x O y/Al2O3 (M= Ni, Fe, Co) heteroaggregate catalysts by in situ transformation of PtM alloy nanoparticles, J. Phys. Chem. C 117 (2013) 7294–7302.
[40] Z. Xu, J. Yu, M. Jaroniec, Efficient catalytic removal of formaldehyde at room temperature using AlOOH nanoflakes with deposited Pt, Appl. Catal. B Environ. 163 (2015) 306–312.
[41] L. Fan, J. Zhao, X. Luo, Z. Tu, Comparison of the performance and degradation mechanism of PEMFC with Pt/C and Pt black catalyst, Int. J. Hydrogen Energy 47 (2022) 5418–5428.
[42] T.W. Patterson, R.M. Darling, Damage to the cathode catalyst of a PEM fuel cell caused by localized fuel starvation, Electrochem. Solid State Lett. 9 (2006) A183.
[43] S. Zhou, T. Tranter, T.P. Neville, P.R. Shearing, D.J. Brett, R. Jervis, Fault diagnosis of PEMFC based on the AC voltage response and 1D convolutional neural network, Cell Reports Physical Science (2022), 101052.